

FOURIER OPTICS

NICHOLAS GEORGE
THE INSTITUTE OF OPTICS

DECEMBER 2012

KEYWORDS

- ELECTROMAGNETIC WAVES
- MAXWELL'S EQUATIONS
- RAYLEIGH, SOMMERFELD, SMYTHE
- RIGHT-HALF-SPACE PROPAGATION
- NON-PARAXIAL OPTICS
- IMPULSE RESPONSE
- PERFECT LENS
- CASCADED LENSES
- ASPHERE LENS
- OPTICAL FOURIER TRANSFORM
- TRANSMISSION FUNCTION
- RING WEDGE PHOTODETECTOR
- EXACT CIRCULAR APERTURE
- 4F OPTICAL PROCESSOR

ngeorge@optics.rochester.edu
Hajim School of Engineering & Applied Science
University of Rochester
Rochester, New York 14627

FOURIER OPTICS
NICHOLAS GEORGE
JOSEPH C. WILSON PROFESSOR OF ELECTRONIC IMAGING
PROFESSOR OF OPTICS
THE INSTITUTE OF OPTICS

Fourier optics: PREFACE

This monograph on Fourier Optics contains a rigorous treatment of this important topic based on Maxwells Equations and Electromagnetic Theory. One need know only the elements of calculus and vector analysis in order to understand the contents of this work. In the emerging field of Image Science it is important in the thinking, creation, design, and understanding of novel or modern optical systems that one consider the input electric field $\mathcal{E}(\mathbf{r}, t)$ and its intensity, proportional to $\mathcal{E} \bullet \mathcal{E}$, and its progress through the complete system. The complete system includes of course the optical front-end, an array-type of photodetector, the computing system, and the output display or function.

Fourier optics is the field of physics that encompasses the study of light at visible wavelengths but including infrared and ultraviolet portions of the electromagnetic spectrum as well. Based upon Maxwell's equations for the electromagnetic field and using modern transform mathematics, principally Fourier transform theory in the solutions, Fourier Optics is particularly well suited to the study of cascades of lenses and phase masks as are widely used in optical instruments ranging from microscopes to telescopes, i.e., linear optical systems. Fourier Optics also incorporates the advances in communication theory in the treatment of coherency topics to permit a rich, full analysis of optical systems that use various sources of illumination ranging from incoherent or white light to modulated laser beams. For Physical Optics, systems study of the point-spread-function and the optical transfer function can be described in a rigorous fashion. General transmission functions for lenses can be formulated and optical-system design that is valid in the non-paraxial regime is now practical. Fourier Optics places the analyses of linear optical systems on a rigorous theoretical foundation enabling one to calculate resolution, imaging and other interference phenomena in a careful and accurate fashion.

This monograph is based on the experience by the author in lecturing on Electromagnetic Waves and Fourier Optics for over forty years to a talented and inspiring group of doctoral scholars at the California Institute of Technology and later at The Institute of Optics, University of Rochester.

– Nicholas George, January 2013, Rochester, New York

FOURIER OPTICS
NICHOLAS GEORGE
JOSEPH C. WILSON PROFESSOR OF ELECTRONIC IMAGING
PROFESSOR OF OPTICS
THE INSTITUTE OF OPTICS

Contents

1	Introduction to electromagnetic waves and Fourier optics	1
1.1	Maxwell's equations in real-valued form	2
1.2	Fourier analysis in three dimensions	3
1.3	Maxwell's differential equations in temporal transform form	3
2	Propagation into the right-half-space	5
2.1	Rayleigh-Sommerfeld-Smythe solution	5
2.2	Impulse response for propagation into the RHS	9
2.3	Summary of impulse response	10
2.3.1	The Right-Half-Space	10
2.3.2	The full 4π -steradian space	11
3	Optical diffraction illustrations	12
3.1	The circular aperture	13
3.2	The far-zone	17
3.2.1	The rectangular aperture	19
3.3	The Fresnel zone	19
4	Transmission function theory for lenses	21
4.1	Review of simple lens models [2]	21
4.2	Generalized transmission function for aspheres	25
4.3	Illustrative design of the tailored asphere	27
4.4	The paraxial approximation for a lens transmission function	30
5	Cascade of lenses & impulse response	30
6	The optical Fourier transform	32
7	The optical transform hybrid processor	33
7.1	The ring-wedge photodetector [16]	35
8	Canonical optical processor - the 4F system	36
9	Summary	40

Copyright © 2012 by Nicholas George,
All rights reserved.

List of Figures

1	Signal representations in Electromagnetic Waves and Fourier Optics	4
2	Radiation into the right-half-space from a circular aperture in the $z = 0$ plane	6
3	Notation in the calculation for Sommerfeld's Green's function with a δ -function at point $r'(x_1, y_1, z_1)$ in the right-half-space.	7
4	Sommerfeld's Green's function in Eq. (23) and integration over the $z = 0$ plane.	7
5	Uniformly illuminated circular aperture of radius (a) is calculated on axis to provide clear picture of (NZ) near field, (FZ) Fresnel zone and the FAR-zone. [10]	13
6	Axial field strength squared $w(z)$ vs $\log(z)$ for uniformly illuminated circular aperture, as in Eq. (51) The dashed lines are the envelope of $w(z)$. The actual value of $w(z)$ is plotted in red in the Fresnel zone for the first few cycles, but it is too fine scalar to plot accurately.	15
7	Convergent lens with R_1, R_2 positive and a positive focal length as in Eq. (70)	22
8	Positive lens with rays (upper) and wavefronts (lower). The converging wavefronts are labelled with phase corresponding to HTD of $\exp(i\omega t)$ dependence	23
9	Notation for plano-convex lens with central thickness H_o . Calculation of phase delay at red ray δ in air and $h(\rho)$ in glass.	24
10	Transmission function for imaging the point source with an asphere, see Eqs. (82) to (85)	26
11	Aspheric lens $\Phi(\rho)$ between planes I - II with plane wave incident. Ray (a) has an effective focal length shown as z.	28
12	Cascade of 4 lenses for imaging input to plane 5. This is a central topic in Fourier optics to compute the impulse response p_{05} for the cascade	31
13	The optical Fourier transform configuration. From two Fresnel zone calculations, one finds an ideal Fourier transform in plane III for the input $E_I(x, y)$.	32
14	The basis of diffraction-pattern-sampling for pattern recognition in optical-electronic processors is summarized in 4 rules	34
15	Rapid, millisecond testing of quality of sharpness of hypodermic needles (2.5 billion needles per year) is accomplished with the ring-sedge optical transform hybrid: (left) excellent quality; poor needle; poor transform.	36
16	The 4-F optical processing provides both an idealized space-invariant image as well as a perfect optical Fourier transform. It is useful both in theoretical calculations and in laboratory.	39

1 Introduction to electromagnetic waves and Fourier optics

The foundations of the subject of Fourier Optics rest on Maxwell's equations, the early studies of interference and interferometry, coherence, and imaging. Important advances in the mathematics of transform theory leading to communication theory from 1900 to the present greatly aided our understanding of these phenomena; the general notion of signal representations such as $\text{HTD } \exp(i\omega t)$ herein, and the Fourier transform for optics, and the Laplace transform for electronic circuits. Professor P. M. Duffieux authored "L'integral de Fourier et ses applications à l'optique", Masson Editeur, Paris, 1970 with first editions going back to the early forties. "It represents the first book-length treatment of what is now called Fourier optics" [1]. At the (1970) meeting of the International Symposium on the applications of Holography (ICO) in Besançon, at a Medal awarding address, Dr. Duffieux told a charming story of how a mathematics professor and colleague had told him about the Fourier transform when PMD showed him some integral forms he had derived in study of the earlier work of Ernst Abbe.

Interestingly the technological advances in monochromatic sources in electronics, particularly radio and microwave from 1900 to 1950 lead to greatly enhanced theoretical studies and many now-classic textbooks, appeared using HTD of amplitudes.

In optics intensity based considerations were more commonly employed. A notable exception is the brilliant advances in coherence theory leading to phase contrast microscopy. However, in Optics this situation changes dramatically with the invention and development of holography and nearly monochromatic lasers. The theoretical treatment and understanding of these novel devices were greatly aided by the appearance of now classic textbooks on Fourier Optics [2, 3].

This article contains a modern complete theoretical treatment of Fourier Optics based on Maxwell's equations and current signal representations, as devised from the subject of communication theory.

1.1 Maxwell's equations in real-valued form

The basic equations of electromagnetic theory are briefly reviewed for a simple linear medium so that the signal representation herein can be carefully explained. In this first section, we describe the time-varying real-valued electric field vector $\mathcal{E}(\mathbf{r}, t)$ and the time-varying magnetic field vector $\mathcal{H}(\mathbf{r}, t)$ in Eq. (1) Faraday's Law and Eq. (2) the generalized Ampere's circuit law including Maxwell's electric displacement term. Undergraduate level derivation of these first six differential equations of electrodynamics and their application across the electromagnetic spectrum appear in many texts, e.g., [4] Griffiths. This article is written using the SI/mks system of units. The time-dependent real-valued functions are related as given in Eqs. (1) through (6):

$$\nabla \times \mathcal{E}(\mathbf{r}, t) = -\frac{\partial \mathcal{B}(\mathbf{r}, t)}{\partial t} \quad (1)$$

$$\nabla \times \mathcal{H}(\mathbf{r}, t) = \mathcal{J}(\mathbf{r}, t) + \frac{\partial \mathcal{D}(\mathbf{r}, t)}{\partial t} \quad (2)$$

$$\nabla \bullet \mathcal{D}(\mathbf{r}, t) = \rho(\mathbf{r}, t) \quad (3)$$

$$\nabla \bullet \mathcal{B}(\mathbf{r}, t) = 0 \quad (4)$$

$$\nabla \bullet \mathcal{J}(\mathbf{r}, t) = -\frac{\partial \rho(\mathbf{r}, t)}{\partial t} \quad (5)$$

$$\nabla \times \nabla \times \mathcal{E}(\mathbf{r}, t) + \mu \varepsilon \frac{\partial^2 \mathcal{E}(\mathbf{r}, t)}{\partial t^2} = -\mu \frac{\partial \mathcal{J}(\mathbf{r}, t)}{\partial t} \quad (6)$$

The field vectors are written in boldface type and the common symbols are used for divergence ($\nabla \bullet$) and curl ($\nabla \times$). Restricting the media to simple dielectrics, the constitutive parameters for permittivity ε and permeability μ also give us

$$\mathcal{B} = \mu \mathcal{H} \quad (7)$$

and
$$\mathcal{D} = \varepsilon \mathcal{E} \quad (8)$$

An exact solution of Maxwell's equations is obtained when one has $\mathcal{E}(\mathbf{r}, t)$ and $\mathcal{H}(\mathbf{r}, t)$ that satisfy Eqs. (1) and (2). Other paths to exact solutions are to obtain $\mathcal{E}(\mathbf{r}, t)$ from Eq. (6) and then use Eqs. (1) and (7) to find $\mathcal{H}(\mathbf{r}, t)$. Finally, one can introduce any of a variety of vector potentials that have been developed for particular cases.

1.2 Fourier analysis in three dimensions

Consider a scalar function $g(x, y, t)$ with two transverse spatial coordinates and one temporal coordinate. Now define the Fourier transform $G(f_x, f_y; \nu)$ by the following equation:

$$G(f_x, f_y; \nu) = \iiint_{-\infty}^{\infty} g(x, y, t) e^{-i2\pi(f_x x + f_y y + \nu t)} dx dy dt \quad (9)$$

It is a straightforward exercise to show that the inversion expression is given by Eq. (10):

$$g(x, y, t) = \iiint_{-\infty}^{\infty} G(f_x, f_y; \nu) e^{i2\pi(f_x x + f_y y + \nu t)} df_x df_y d\nu \quad (10)$$

This notation and sign convention is used throughout this paper. It is particularly convenient since the sign of the exponents in the transform kernel are all negative while those of the inversion are all positive.

1.3 Maxwell's differential equations in temporal transform form

In Sec. 1.2, the notation for Fourier analysis in three dimension has been presented in order to place in evidence the sign convention to be used. Now, however, we use the obvious form for the temporal transform alone, since we wish to compare the resulting equations to "standard" HTD expressions.

Important integral solutions of Maxwell's equations are readily obtained using temporal Fourier transform forms of Eqs. (1) (2) and (6) with the corresponding results in Eqs. (11) , (12) and (13) , (14) directly below:

$$\nabla \times \mathbf{E}(\mathbf{r}; \nu) = -i\omega\mu\mathbf{H}(\mathbf{r}; \nu) \quad (11)$$

$$\nabla \times \mathbf{H}(\mathbf{r}; \nu) = \mathbf{J}(\mathbf{r}; \nu) + i\omega\epsilon\mathbf{E}(\mathbf{r}; \nu) \quad (12)$$

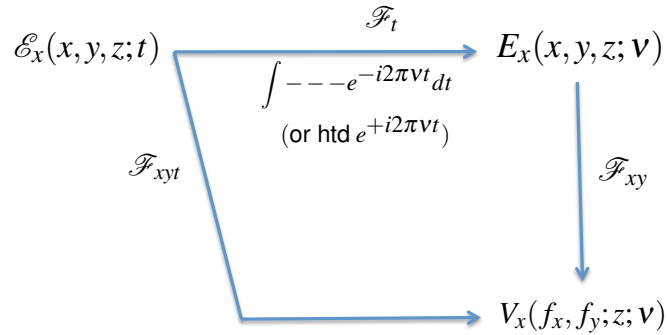
$$\nabla \times \nabla \times \mathbf{E}(\mathbf{r}; \nu) - \omega^2\mu\epsilon\mathbf{E}(\mathbf{r}; \nu) = -i\omega\mu\mathbf{J}(\mathbf{r}; \nu) \quad (13)$$

$$(\nabla^2 + k^2)\mathbf{E}(x, y, z) = 0 \quad (14)$$

Equation (14) is valid in a source free region.

Now these temporal transform equations are exact and rigorous for optical sources which are transient. Since temporal frequency ν is a variable, solving the above equations gives us a new path to solving problems in which there are broadband sources or multi-tone spectra.

$$\begin{aligned} \nabla \times \mathcal{E} &= -\frac{\partial \mathcal{B}(\mathbf{r}, t)}{\partial t} & \nabla \times \mathbf{E} &= -i2\pi\nu\mathbf{B} \\ \nabla^2 \mathcal{E}_x &= \mu\epsilon \frac{\partial^2 \mathcal{E}_x}{\partial t^2} & (\nabla^2 + k^2)E_x(x, y, z; \nu) &= 0 \end{aligned}$$



$$\begin{aligned} \frac{\partial^2 V_x}{\partial z^2} + [k^2 - (2\pi f_x)^2 - (2\pi f_y)^2] V_x &= 0 \\ V_x(f_x, f_y; z; \nu) &= \iint_{-\infty}^{\infty} dx dy E_x(x, y, z; \nu) e^{-i2\pi f_x x - i2\pi f_y y} \\ E_x(x, y, z; \nu) &= \iint_{-\infty}^{\infty} df_x df_y V_x(f_x, f_y; z; \nu) e^{+i2\pi f_x x + i2\pi f_y y} \end{aligned}$$

Figure 1: Signal representations in Electromagnetic Waves and Fourier Optics

In order to place emphasis on the significance of the result to be inferred from Eqs. (11) through (14), let us observe that Eqs. (11) and (12) are simply and precisely the harmonic-time-dependence differential equations for an electromagnetic wave. The reader is cautioned, however, that our Eq. (9) notation is consistent with an $\exp(i\omega t)$ as in ref. [6].

In Fig. 1 we show the signal representations being used in Sections 1.1 and 1.2 in more detail than is necessary for the paper at hand. However, we wanted to show the more general usage including angular spectrum as well as statistical optics in order to explain our preference for the $\exp(+i\omega t)$

in the HTD representation and its consistency with our Fourier transform notation.

2 Propagation into the right-half-space

Maxwell's equations give us the means to obtain exact solutions of many optics problems. Both the Hertzian electric dipole and the magnetic dipole are significant and important and covered in many textbooks [5] - [7]. In optics, diffraction theory topics such as propagation through screens, slits, and various apertures were studied extensively for several hundred years. Also lens trains formed by a cascade of lenses along an optical axis is a common configuration, as in Sec. 5.

2.1 Rayleigh-Sommerfeld-Smythe solution

Consider a monochromatic electromagnetic wave traveling along the optic z -axis and incident on an aperture as in Fig. 2. This is a classic problem in the propagation of waves since the time of Francesco Grimaldi and Christiaan Huygens.

We assume there are sources of radiation only in the region $z < 0$ and that we have knowledge of the "field" in the aperture. The radiation propagates into the right-half-space which is a simple source-free region. Viewed with today's understanding, as will be shown, if one views this as a boundary-value problem, there will be an exact integral form of the radiation at $z > 0$ for $\mathcal{E}(\mathbf{r}, t)$ and $\mathcal{H}(\mathbf{r}, t)$ that converges to the given tangential electric field $\hat{z} \bullet \mathcal{E}(\mathbf{r}, t)$. As is illustrated by the solution, the tangential input electric field at $z = 0$ is the necessary and sufficient input specification, as recognized first by Sommerfeld for the HTD case.

Now to obtain the desired solution for radiation in the right-half-space one starts with Eq. (14) rewritten for each Cartesian component, viz.,

$$\nabla^2 E_x(x, y, z) + k^2 E_x = 0 \quad (15)$$

$$\nabla^2 E_y(x, y, z) + k^2 E_y = 0 \quad (16)$$

$$\nabla^2 E_z(x, y, z) + k^2 E_z = 0 \quad (17)$$

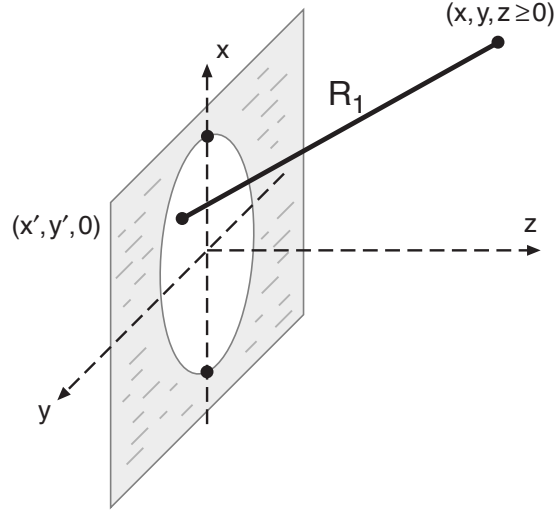


Figure 2: Radiation into the right-half-space from a circular aperture in the $z = 0$ plane

Now consider the use of a Green's function solution using either Eq. (15) or (16), as follows. We write

$$G_s(\nabla^2 + k^2)E_x = 0 \quad (18)$$

$$E_x(\nabla^2 + k^2)G_s = -\delta(\mathbf{r} - \mathbf{r}')E_x \quad (19)$$

where \mathbf{r}' is at $(x_1, y_1, z_1 \geq 0)$ in the right-half-space, as shown in Fig. 3 and the vector operations are at the point $\mathbf{r}(x, y, z)$. Moreover, the Green's function $G_s(x, y, z; x_1, y_1, z_1)$ has a singularity at \mathbf{r}' . Forming the difference of Eqs. (18) and (19) and integration over the right-half-volume and using Green's second identity yield the following intermediate result:

$$E_x(x_1, y_1, z_1) = \iint_{RHS} (G_s \nabla E_x - E_x \nabla G_s) \cdot \hat{\mathbf{n}}_{out} dA \quad (20)$$

Sommerfeld broke this integration in Eq. (20) into parts asserting that the integral over the hemisphere in the far zone goes to zero for a finite

aperture source (see Eq. (22) below).

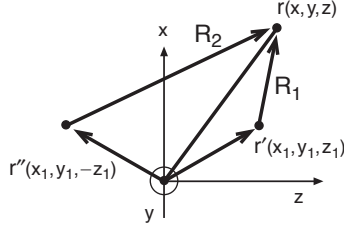


Figure 3: Notation in the calculation for Sommerfeld's Green's function with a δ -function at point $r'(x_1, y_1, z_1)$ in the right-half-space.

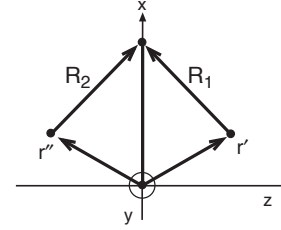


Figure 4: Sommerfeld's Green's function in Eq. (23) and integration over the $z = 0$ plane.

The integration over the plane at $z = 0$ has two members by a proper choice of the Green's function G_s , one can zero out the first member of the integration over the $z = 0$ plane, regardless of the non-zero value of ∇E_x there. Hence by Eq. (18), the scalar component E_x for $z \geq 0$ is given by

$$E_x(x_1, y_1, z_1 \geq 0) = \iint_{z=0} E_x \nabla G_s \bullet \hat{\mathbf{z}} \, dx dy \quad (21)$$

Moreover summarizing, one has the Sommerfeld radiation condition that the term $S \rightarrow 0$ where S is given by

$$S = \iint_{R_1 \rightarrow \infty} (G_s \nabla E_x - E_x \nabla G_s) \bullet \hat{\mathbf{r}} \, dA \rightarrow 0. \quad (22)$$

Also, the appropriate choice for $G_s(x, y, 0; x_1, y_1, z_1)$ is given by

$$G_s = \frac{e^{-ikR_1}}{4\pi R_1} - \frac{e^{-ikR_2}}{4\pi R_2} \quad (23)$$

in which

$$R_1 = [(x - x_1)^2 + (y - y_1)^2 + (z - z_1)^2]^{1/2} \quad (24)$$

and $R_2 = [(x - x_1)^2 + (y - y_1)^2 + (z + z_1)^2]^{1/2}. \quad (25)$

In Figs. 3 and 4, one sees that placing r'' as the image point of r' in the z -plane establishes that $G_s(x, y, 0; x_1, y_1, z_1) = 0$ in the $z = 0$ plane as required to drop out the term in the integral regardless of the value of ∇E_x .

Thus, the Green's function choice by Sommerfeld in Eq. (23) is the key to finding an exact solution for E_x in the right-half-space.

A straightforward algebraic calculation on $G_s(x, y, z; x_1, y_1, z_1)$ for

$$\nabla G_s \bullet \hat{\mathbf{z}} = \left. \frac{\partial G_s}{\partial z} \right|_{z=0} \quad (26)$$

leads to the important result:

$$\left. \frac{\partial G_s}{\partial z} \right|_{z=0} = \frac{e^{-ikR_1}}{2\pi R_1} \left(ik + \frac{1}{R_1} \right) \frac{z_1}{R_1}. \quad (27)$$

Substitution of Eq. (27) into Eq. (21) yields the desired result for the interior scalar electric field component, namely

$$E_x(x_1, y_1, z_1 \geq 0) = \iint_{-\infty}^{\infty} dx dy E_x(x, y, 0) \frac{e^{-ikR_1}}{2\pi R_1} \left(ik + \frac{1}{R_1} \right) \frac{z_1}{R_1} \quad (28)$$

in which the distance R_1 is given exactly by Eq. (24).

Now, typical of Green's function solutions, we make a change in coordinates in Eq. (28) in order to have the aperture point labeled $(x', y', 0)$ and the interior RHP point (x, y, z) as in Fig. 2. The result of this relabeling in coordinates leads to the desired final form for

$$E_x(x, y, z \geq 0) = \iint_{-\infty}^{\infty} dx' dy' E_x(x', y', 0) \frac{e^{-ikR_1}}{2\pi R_1} \left(ik + \frac{1}{R_1} \right) \frac{z}{R_1} \quad (29)$$

and of course now R_1 in Eq. (29) becomes

$$R_1 = [(x - x')^2 + (y - y')^2 + (z - 0)^2]^{1/2}. \quad (30)$$

One can complete this derivation by stating that this result can also be written for $E_y(x, y, z \geq 0)$. Now using $\nabla \bullet \mathbf{E}(x, y, z; \nu) = 0$, we can find an expression for E_z that stresses its dependence on E_x and E_y . We omit the details of this calculation until later in Eq. (35) since there is much more to write about these results using an independent approach in Sec. 2.2 below.

2.2 Impulse response for propagation into the RHS

In linear optical systems a topic of central interest is to derive an exact impulse response for propagation into the right-half-space (RHS). In Sec. 2.1 Eq. (29) is presented as a rigorous solution of Maxwell's equation for this impulse response. It is applicable over the entire range that Maxwell's equations holds from near field optics to telescopes. Hence, in this article it seemed worthwhile to develop an independent derivation of Eq. (29) and related material.

Again consider the setup and notation in Figs. 2 for radiation into the RHS. Smythe was at least early to write out a detailed existence theorem for electromagnetic waves in a closed source-free region, and he stressed the necessary and sufficient need for either the tangential electric field or the tangential magnetic field, although he did not explicitly cover a region such as the RHS [8]. Also Smythe was first to write the complete exact solution for the right-half-space problem in an entirely vector form in his famous Phys. Rev. (1947) paper [9]. The vector result for the internal field is given in Fourier optics or HTD form as follows:

$$\mathbf{E}(\mathbf{r}; \nu) = \frac{1}{2\pi} \nabla \times \iint_{z'=0} \hat{z}' \times \mathbf{E}(\mathbf{r}') \frac{e^{-ikR_1}}{R_1} dx' dy' \quad (31)$$

in which the free-space Green's function G is appropriate as follows:

$$G(\mathbf{r}, \mathbf{r}') = \frac{e^{-ikR_1}}{4\pi R_1}, \quad (32)$$

and $\mathbf{E}(\mathbf{r}')$ at $(x', y', 0)$ is the final field in the aperture.

Let me describe some illuminating illustrative exercises for the dedicated reader. Derive the equations below in Eq. (33) to (35) for the components.

To verify that this result in Eq. (31) is an exact solution for Maxwell's equations, one needs to verify that the vector $\mathbf{E}(\mathbf{r}; \nu)$ is a solution of the vector wave equation (13) or (14).

It is fascinating to see the impulse responses for propagation into the RHS for a simple medium. There is no "mixing" of the x and y polarizations. Moreover, both the E_x and E_y are seen to contribute to the E_z component. This illustrates very nicely the existence theorem for this situation

and Maxwell's equations. For the RHS problem, one can supply any reasonable functions for the tangential components E_x and E_y (necessary and sufficient) but any more will likely lead to inconsistent results.

2.3 Summary of impulse response

2.3.1 The Right-Half-Space

Here are the exact solutions of Maxwell's equations for propagation in the right-half-space.

The Rayleigh-Sommerfeld-Smythe formulas:

$$E_x(x, y, z) = \iint_{-\infty}^{\infty} dx' dy' E_x(x', y', 0) \frac{e^{-ikR_1}}{2\pi R_1} \left(ik + \frac{1}{R_1} \right) \frac{z}{R_1} \quad (33)$$

$$E_y(x, y, z) = \iint_{-\infty}^{\infty} dx' dy' E_y(x', y', 0) \frac{e^{-ikR_1}}{2\pi R_1} \left(ik + \frac{1}{R_1} \right) \frac{z}{R_1} \quad (34)$$

$$E_z(x, y, z) = \iint_{-\infty}^{\infty} dx' dy' \left\{ E_x(x', y', 0) \frac{x' - x}{R_1} + E_y(x', y', 0) \frac{y' - y}{R_1} \right\} \frac{e^{-ikR_1}}{2\pi R_1} \left(ik + \frac{1}{R_1} \right) \quad (35)$$

Another exact, useful and readily proven result for the RHS is given by [10]:

$$E_{x,y}(x, y, z) = -\frac{\partial}{\partial z} \iint_{-\infty}^{\infty} dx' dy' E_{x,y}(x', y', 0) \frac{e^{-ikR_1}}{2\pi R_1} \quad (36)$$

They are valid for $z \geq 0$, and R_1 is given by Eq. (30), Fig. 2.

Many scientists have contributed to an understanding of interference patterns arising as light propagates, e.g., from two pinholes, through an open aperture, or from an array of coherent sources. Huygens' principle stated more than three hundred years ago in the description of the propagation of a wavefront is among the earliest major contributions. His assertions are in accord with the theory which we have presented.

For us, today, using Maxwell's equations and the formula presented on the previous page, we can see that a diffraction pattern is made up by the

superposition of radiation from differential elements given by

$$dx' dy' E_x(x', y', 0).$$

These give rise to “secondary waves” which are traveling in the right-half-space with a very weak angular dependents given by the term z/R_1 . The superposition weighting is given precisely in amplitude and phase by the term:

$$\frac{e^{-ikR_1}}{2\pi R_1} \left(ik + \frac{1}{R_1} \right) \frac{z}{R_1}$$

All of the physical details of interference patterns are contained in these formulas for the radiation in the right-half-space resulting from a given aperture distribution.

2.3.2 The full 4π -steradian space

In the classic text on electromagnetic wave by Papas [5], there is an excellent treatment of radiation from monochromatic sources in unbounded regions, i.e., 4π steradians. He describes two methods of solution: vector potentials and the dyadic Green’s function. While our emphasis for optics is on the right-half-space topic, it is important to mention this basic result for the impulse response for the 4π -steradian or full-space case.

For the same simple medium with constitutive parameters μ , ε , one has the same group of Maxwell’s equations as our Eqs. (11), (12).

The magnetic vector potential \mathbf{A} is defined by

$$\mathbf{B} = \nabla \times \mathbf{A}. \quad (37)$$

Hence, by Eq. Eq. (11), one can write the \mathbf{E} field as

$$\mathbf{E} = -i\omega\mathbf{A} - \nabla\phi. \quad (38)$$

With the choice of the Lorenz gauge relating \mathbf{A} and ϕ , namely that

$$\nabla \bullet \mathbf{A} + i\omega\varepsilon\mu\phi = 0 \quad (39)$$

one can write a wave equation as follows:
for the vector potential $\mathbf{A}(\mathbf{r}; \nu)$:

$$\nabla^2 \mathbf{A} + k^2 \mathbf{A} = -\mu \mathbf{J}. \quad (40)$$

Presenting a Green's function solution, Papas derives the integral equation solution for the radiation into free space, 4π -steradians:

$$\mathbf{A}(\mathbf{r}) = \iiint_{-\infty}^{\infty} dx' dy' dz' J(\mathbf{r}') \frac{e^{-ikR_1}}{4\pi R_1} \quad (41)$$

Equation (41) is the basis equation for radiation of electromagnetic waves into free space in a spherical configuration. It is particularly useful for radiation of current sources as given by $\mathbf{J}(\mathbf{r}', \nu)$ where the R_1 is given by

$$R_1 = [(x - x')^2 + (y - y')^2 + (z - z')^2]^{1/2} \quad (42)$$

It is important to understand these two distinct radiation problems. They are often confused. First, one has the scalar electric field components propagating into the right-half-space expressed in terms of source-terms in the plane at $z = 0$. The solutions are given in Eqs. (33) to (36).

Secondly, in the radiation into 4π -space, we have the vector potential $\mathbf{A}(\mathbf{r}; \nu)$ resulting from source currents $\mathbf{J}(\mathbf{r}'; \nu)$, and the resulting impulse response given by the free-space Green's function in Eq. (41).

3 Optical diffraction illustrations

The theory of Fourier Physical Optics as presented in the earlier sections of this article is based on Maxwell's equations. The precision possible with rigorous or exact solutions of electromagnetic theory is discussed in some detail in Jackson [11]. This enormous range includes wavelength or frequency from fractional cycles per second to ultraviolet and of course DC. It includes power range from 10^{-20} watts to many megawatts. It also includes subpulse propagation as well as $\mu\mu\text{sec}$ transients. Many new fields

are developing in optics such as computational imaging that are permitting the solution of many boundary value problems, and near-field optics problems that were considered inaccessible until rather recently.

3.1 The circular aperture

For a first illustration, it is helpful to start with an important problem in which a theoretical approach leads to interesting results [10]. Consider a perfectly conducting, infinitesimally thin conducting plane sheet containing a circular aperture of radius (a) placed in the (x,y) plane at $z = 0$, as shown in Fig. 5. It is illuminated by a plane-polarized monochromatic plane wave with wave number $k = 2\pi/\lambda$ where $\lambda \ll a$ so boundary effects can be ignored. Clearly, Eq. (33) or (36) can be used. Let us restrict our solution to the optic axis z so that we gain an understanding of the different zones shown. Hence, for a fixed amplitude E_o of the scalar component of electric field, by Eq. (36), one can write the field along the optical axis $E_x(0, 0, z; \nu)$ as

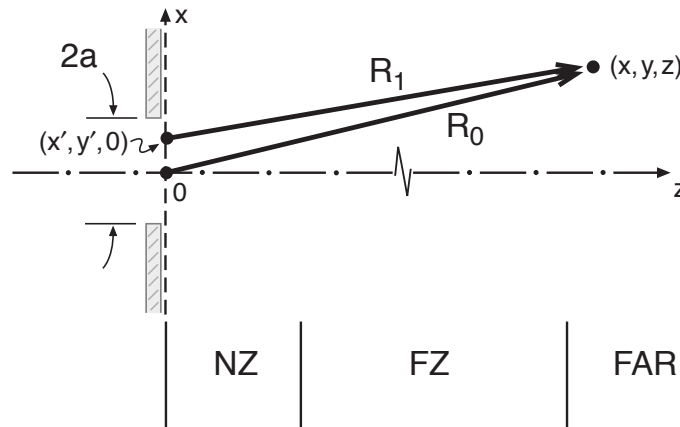


Figure 5: Uniformly illuminated circular aperture of radius (a) is calculated on axis to provide clear picture of (NZ) near field, (FZ) Fresnel zone and the FAR-zone. [10]

$$E_x(0,0,z \geq 0) = -\frac{\partial}{\partial z} \iint_A dx' dy' E_x(x',y',0) \frac{e^{-ikR_1}}{2\pi R_1}, \quad (43)$$

in which the illumination is given in polar coordinates, viz.

$$E_x(x',y',0) = E_o \text{circ}(\rho/a), \quad \rho = [x'^2 + y'^2]^{1/2} \quad (44)$$

and the distance R_1 given in polar form is

$$R_1 = [\rho^2 + z^2]^{1/2}. \quad (45)$$

Equation (43) is rewritten to yield:

$$E_x(0,0,z \geq 0) = -E_o \frac{\partial}{\partial z} \int_0^a \frac{e^{-ik(\rho^2 + z^2)^{1/2}}}{(\rho^2 + z^2)^{1/2}} 2\pi\rho d\rho. \quad (46)$$

This can be integrated exactly to yield the result:

$$E_x(0,0,z \geq 0) = E_o \left\{ e^{-ikz} - \frac{z}{d} e^{-ikd} \right\} \quad (47)$$

where

$$d = \sqrt{a^2 + z^2}. \quad (48)$$

First as expected, when $z \rightarrow 0$, the radiation field at the aperture reduces to the input E_o . As described in Sec. 2.2, this result is consistent with the existence theorem for Maxwell's equations, Eqs. (1) through (4), extended to the right-half-space and adding Sommerfeld radiation condition, given by Eq. (22). We see that specification of HTD together with the tangential electric field at the input plane $z = 0$.

By Eq. (34) one sees that $E_y(x,y,z \geq 0)$ is identically zero as expected. And of course, one can calculate E_z by Eq. (35) clearly dependent on the non-zero tangential electric field, E_x , input.

In order to study the z -dependence of E_x further, it is interesting to think of the calculation as in the HTD signal representation. By Eqs. (47) and (48), one can insert the time dependence simply as follows:

$$E_x(0,0,z;t) = E_o \left\{ e^{-ikz} - \frac{z}{\sqrt{z^2 + a^2}} e^{-ik\sqrt{z^2 + a^2}} \right\} e^{+i2\pi\nu t}. \quad (49)$$

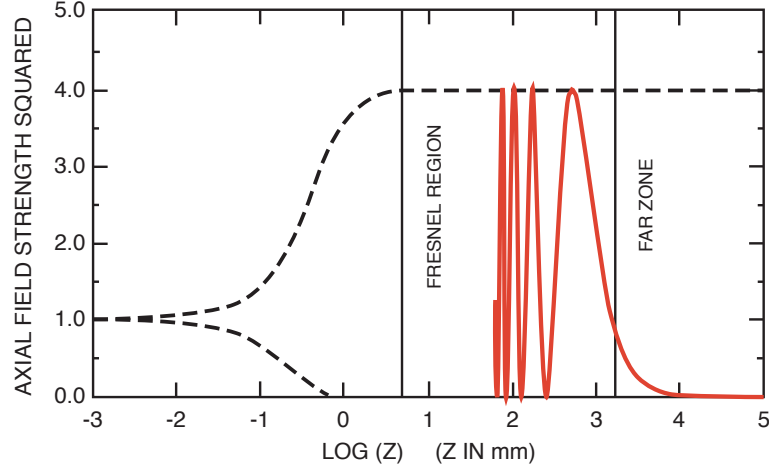


Figure 6: Axial field strength squared $w(z)$ vs $\log(z)$ for uniformly illuminated circular aperture, as in Eq. (51) The dashed lines are the envelope of $w(z)$. The actual value of $w(z)$ is plotted in red in the Fresnel zone for the first few cycles, but it is too fine scalar to plot accurately.

In order to monitor the optical field along the optical axis, one can use a single photodiode or a CMOS detector array. Hence, in our illustrative study, we will use energy density in the E_x electric field. Hence, we define w as follows

$$w(z) = |E_x(0, 0, z : t)|^2. \quad (50)$$

Hence combining Eq. (47) and (48) with some algebra yields the following form:

$$w(z) = |E_o|^2 \left\{ 1 + \frac{z^2}{z^2 + a^2} - 2 \frac{z}{\sqrt{z^2 + a^2}} \cos k[\sqrt{z^2 + a^2} - z] \right\} \quad (51)$$

in which $k = 2\pi/\lambda$.

No approximations have been made in deriving Eq. (51) for the squared electric field component E_x from the initial solution in Eq. (47). Hence, it is

useful as an illustration, and it is plotted in Fig. 6.

The plot shows Eq. (51) for $w(z)$ vs. z in mm. The aperture diameter $2a = 1$ mm and the optical wavelength $\lambda = 0.5 \mu\text{m}$. The envelope for $w(z)$ is plotted as the dashed lines since the amplitude variations in the optical field are tiny compared to the z -axis mm scale.

This theoretical problem provides a lovely illustration of the main radiation zones that are so important in diffraction problems. Here we would like to point out that the far-zone or Fraunhofer zone start at roughly 1 meter for the one-millimeter aperture. And in this region, the electric field falls off as $1/z$ while the intensity falls off as $1/z^2$.

Coming in closer, one sees the natural occurrence of another zone called the Fresnel zone, treated in Sec. 3.3 below. Looking at the scale in Fig. 6, the Fresnel zone comes to an end at about 6 mm. If one goes in closer, the calculations become very difficult to carry out in closed form if one goes off-axis. However, they are nicely handled with modern digital computers and computational imaging.

From Eqs. (33) and (35) as well as the discussion of Eq. (38) for the impulse response of the right-half-space, it is appropriate to discuss the new field of computational optics. Viewing the main equations for the right-half-space, we have emphasized the notion that the interior that the interior fields in a closed volume with no internal sources can be calculated from a knowledge, say, of the tangential component of the electric field (necessary and sufficient). From the illustration of the simple circular aperture, Fig. 6, one clearly sees the field $E_x(0,0,z)$ converges to the input tangential field, E_o . This is generally true for all of the RHP forms.

For near-field optics it is interesting to take note of the two members of the amplitude impulse response:

$$p(x,y;x',y';\nu) = \frac{e^{-ikR_1}}{2\pi R_1} \left(ik + \frac{1}{R_1} \right) \frac{z}{R_1} \quad (52)$$

It is important to notice that the $1/R_1$ term will be dominant in the overall integration whenever

$$\begin{aligned} |(1/R_1)/(ik)| &\gg 1 \\ kR_1 &\ll 1 \\ R_1 &\ll \lambda/8. \end{aligned} \quad (53)$$

In the illustration of the circular aperture, of course both terms are included in the calculation. An advanced and comprehensive treatment of the theory of diffraction is provided by Born and Wolf [12].

3.2 The far-zone

Now starting with a more general aperture shape in the $z = 0$ plane of Fig. 2, we consider that an x -plane polarized scalar electric field $E_x(x', y', 0; \nu)$ is used as the illustration. Hence, we seek an approximate, more integrable form of the exact Eq. (33) that is repeated as Eq. (54), i.e.,

$$E_x(x, y, z; \nu) = \iint_{-\infty}^{\infty} dx' dy' E_x(x', y', 0) \frac{e^{-ikR_1}}{2\pi R_1} \left(ik + \frac{1}{R_1} \right) \frac{z}{R_1} \quad (54)$$

The far-zone, also known as the Fraunhofer region, is characterized by large values of R_1 . Mainly in this treatment, we would like carefully to point out the conventional theoretical assumptions in the integration of Eq. (33) or (54) in the far-zone region.

In the far-zone calculation, however, the situation is vastly different relative to accuracy for $\exp(-ikR_1)$. The phase term needs to be accurate to the order of $\pm\pi/8$ no matter how large R_o is. For example, if you are making measurements at 10 m with an optical wavelength of $0.5 \mu\text{m}$, the kR_o is the order of $4\pi \times 10^7$ radians; and the tolerance error in R_1 is fractionally well below one part in 10^7 .

Hence, in the far-zone, Eq. (54) can be approximated by

$$E_x(x, y, z; \nu) = \frac{ik}{2\pi R_o} \left(\frac{z}{R_o} \right) \iint_{-\infty}^{\infty} dx' dy' E_x(x', y', 0) e^{-ikR_1} \quad (55)$$

For the illustration problem, consider an open rectangular aperture that is L_x by L_y length in the conducting metallic sheet at $z = 0$. We take $L_{x,y} > \lambda$ so that we can study the patterns from slits to large square apertures. Using the notation in Fig. 5, we already understand that the distance $R_o \gg \lambda$ so only the ik member in Eq. (54) remains for the far-zone.

Moreover, amplitude terms that are approximated in this integration will cause errors in percentage that are roughly that of the approximation. Hence if a five-percent accuracy solution is sought, then amplitude terms need only be accurate to five-percent.

For the R_1 in the phase term $(-ikR_1)$, we write

$$R_1^2 = [(x-x')^2 + (y-y')^2 + (z-0)^2]^{1/2} \quad (56)$$

Since the far-zone term is often used for telescopes, it is useful to have the expansion valid for large angles θ where

$$\frac{z}{R_o} = \cos \theta \quad (57)$$

is recognized as the spherical angle coordinate.

Hence, one factors out $R_o = (x^2 + y^2 + z^2)^{1/2}$ in the expansion of Eq. (56). For the Fraunhofer zone, the resulting expression for the distance R_1 is approximated by the following:

$$R_1 \cong R_o - \frac{xx' + yy'}{R_o}, \quad (58)$$

$$R_o \gg \frac{2x'^2}{\lambda} \quad \text{all cases of coordinates,} \quad (59)$$

$$E_{x,y}(x,y,z) = \frac{ie^{-ikR_o}}{\lambda R_o} \left(\frac{z}{R_o}\right) \iint_{-\infty}^{\infty} dx' dy' E_{x,y}(x',y',0) e^{i2\pi\left[\left(\frac{x}{\lambda R_o}\right)x' + \left(\frac{y}{\lambda R_o}\right)y'\right]} \quad (60)$$

In Eq. (60) the integration is only over the aperture and this is included as a blocking function in the scalar input field $E_{x,y}(x',y',0)$. It is customary in Fourier optics to write the limits of integration as running over $\pm\infty$. Hence in a cascaded system in which there are many integrals running from $\pm\infty$, and this is to emphasize that the order of integration can be interchanged. This is a key factor in many calculations.

Noting that the exponent in Eq. (60) is of the form of a Fourier transform in which the spatial frequency variables are (f_x, f_y) , one can rewrite Eq. (60) in the following form:

$$E_{x,y}(x,y,z) = \frac{ie^{-ikR_o}}{\lambda R_o} \left(\frac{z}{R_o}\right) \iint_{-\infty}^{\infty} dx' dy' E_{x,y}(x',y',0) e^{-i2\pi[f_x x' + f_y y']}, \quad (61)$$

in which the spatial frequency variables (f_x, f_y) are defined by

$$\begin{aligned} f_x &= -\frac{x}{\lambda R_o} \quad \text{and} \\ f_y &= -\frac{y}{\lambda R_o}. \end{aligned} \quad (62)$$

It is interesting to use Eq. (59) to estimate the axial distance for which the above calculation is valid. Assume that the rectangle in the $z = 0$ plane is on the order of 1 mm and that $\lambda = 0.5\mu\text{m}$. Then, Eq. (59) gives $R_o > 4\text{m}$ as the starting point for the far-zone. This is nicely in accord with our discussion in connection with the Fig. 6 curve showing somewhat over 1 meter for the circular aperture.

Moreover, we also clearly see the $1/R_o$ fall off of the electric field corresponding to an inverse R^2 power.

Moreover, the error in the phase term involved in the exponent can be shown to be a maximum at the $\theta = 0$ angle, decreasing as the angle increases. So factoring out the R_o in the derivation of Eq. (60) is imperative so that Eq. (58) is good at all angles in the right-half-space; i.e., it is not paraxially limited.

3.2.1 The rectangular aperture

For the rectangular aperture L_x by L_y in length Eq. (60) can be integrated directly to yield the following far-zone radiation pattern:

$$E_x(x, y, z) = \frac{ie^{-ikR_o}}{\lambda R_o} \left(\frac{z}{R_o}\right) L_x L_y \frac{\sin\left(\frac{\pi x L_x}{\lambda R_o}\right)}{\left(\frac{\pi x L_x}{\lambda R_o}\right)} \frac{\sin\left(\frac{\pi y L_y}{\lambda R_o}\right)}{\left(\frac{\pi y L_y}{\lambda R_o}\right)}. \quad (63)$$

Or in Fourier optics notation, one has

$$E_x(x, y, z) = \frac{ie^{-ikR_o}}{\lambda R_o} \left(\frac{z}{R_o}\right) L_x L_y \text{sinc}(f_x x) \text{sinc}(f_y y). \quad (64)$$

3.3 The Fresnel zone

In Sec. 3.1 the illustration of the axial field behavior in the right-half-space using a circular aperture showed us that there is a near zone, followed by

a Fresnel zone, and then at larger distances the far-zone. In Sec. 3.2 for the far-zone, we illustrated the theory and a careful calculation that was demonstrated to be good in the right-half-space when the overall range distance $R_o \gg 2x^2/\lambda$. Numerically, we estimated that for small millimeter apertures, one can calculate accurate patterns when $R_o \gtrsim 4$ m. We asserted that the calculation is excellent at all angles. This calculation is an easy extension of the material presented.

However, one very important calculation in Fourier optics is to treat lenses, either a single lens or a cascade of lenses. In this Sec. 3.3 we describe the Fresnel-zone calculation. It is very important since it can be used to handle lens cascades where the spacing is generally much smaller than in the far-zone. As shown for the circular aperture, Figs. 5 and 6, hopefully we are dealing with several millimeters rather than meters.

For the Fresnel zone, the theory proceeds as in Sec. 3.2. First for Eq. (33), we need to establish an expansion for the phase term. Using the notation as in Fig. 5, the exact expression for the distance R_1 is given by

$$R_1 = [(x - x')^2 + (y - y')^2 + (z - 0)^2]^{1/2}. \quad (65)$$

Factoring z and using the binomial expansion gives the following form:

$$R_1 \cong z + \frac{(x - x')^2 + (y - y')^2}{2z}. \quad (66)$$

Factoring with removal of z and leaving (x, y) in the series limits one to a paraxial solution. It is better, however, with regard to axial distance, i.e., valid much closer-in. The limitation on primed coordinates (all cases) is characterized by the following:

$$z^3 \gtrsim \frac{(x - x')^4}{2\lambda}. \quad (67)$$

For a 1 mm aperture, this gives an axial distance $z \approx 10$ mm when $\lambda = 0.5\mu\text{m}$. For the Fresnel zone case, Eq. (33) can be rewritten as

$$E_x(x, y, z; \nu) = \frac{iz}{\lambda R_0^2} \iint_{-\infty}^{\infty} dx' dy' E_x(x', y', 0) e^{-ikR_1}, \quad (68)$$

$$E_x(x, y, z; \nu) = \frac{ie^{-ikz}}{\lambda z} \iint_{-\infty}^{\infty} dx' dy' E_x(x', y', 0) e^{-\frac{i\pi}{\lambda z} [(x-x')^2 + (y-y')^2]}. \quad (69)$$

In many instances of lens design using modern digital computers, one can use Eq. (68) with the exact exponential. However, Eq. (69) is the standard form for a Fresnel calculation. The reader is left to use Eq. (67) to predict the starting point for the Fresnel zone region comparing this estimate to the exact values of the axial field strength as in Fig. 6 from Eq. (51).

4 Transmission function theory for lenses

4.1 Review of simple lens models [2]

Most of the theory relative to the right-half-space topic is concerned with how wavefronts propagate in this region. However, one of the central problems in Fourier optics is to analyze a cascade of lenses that have been placed along an optical axis, say, for the formation of an image or to describe a compound lens. It is important to develop an understanding of the operation of lenses and an analytical theory that is useful for wavefronts. Clearly, too, there is a considerable theory about the design and performance of lenses, since they date back to our earliest history. We are careful in the following material to use sign conventions and language that is consistent with usage in the field of geometric optics, i.e., first-order or Gaussian optics. Our simple cases are to have light traveling from left to right in the positive z -axis direction. Convergent lenses have a positive focal length f . A glass lens with index of refraction n and two positive radii is shown in Fig. 7.

A simple thin lens of glass with index of refraction n will have a focal length f given by

$$\frac{1}{f} = (n-1) \left(\frac{1}{R_1} - \frac{1}{R_2} \right), \quad (70)$$

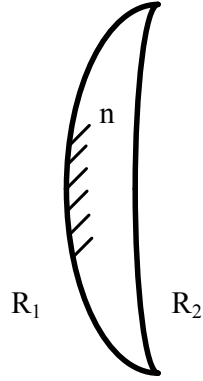


Figure 7: Convergent lens with R_1, R_2 positive and a positive focal length as in Eq. (70)

where R_1 and R_2 are radii of spherical end segments, and the lens is used in air.

Also a point source at s_1 in front of the lens will be imaged at a distance s'_1 given by the lensmaker's equation:

$$\frac{1}{s} + \frac{1}{s'_1} = \frac{1}{f}. \quad (71)$$

Now in order to bring wavefronts into the picture, as shown in red in Fig. 8, consider a plane wave entering the lens which is thicker at the optic axis than at its edges. For a lens that has a spherical segment, the exiting wavefronts will bend forward as shown. Now the phase delay of the plane wave between planes I and II can be calculated approximately by summing $\sum kl$ in a straight ray through the plano-convex structure shown having positive radius R_1 at plane I and an infinite radius at the plane II exit.

Now defining the amplitude transmission function, $T_{12}(\rho)$, as follows:

$$T_{12}(\rho) = \frac{\text{Scalar electric field exiting (II)}}{\text{Scalar electric field entering (I)}} \quad (72)$$

or

$$T_{12}(\rho) = e^{-i\Phi_1}, \quad (73)$$

we can sum the phase delays:

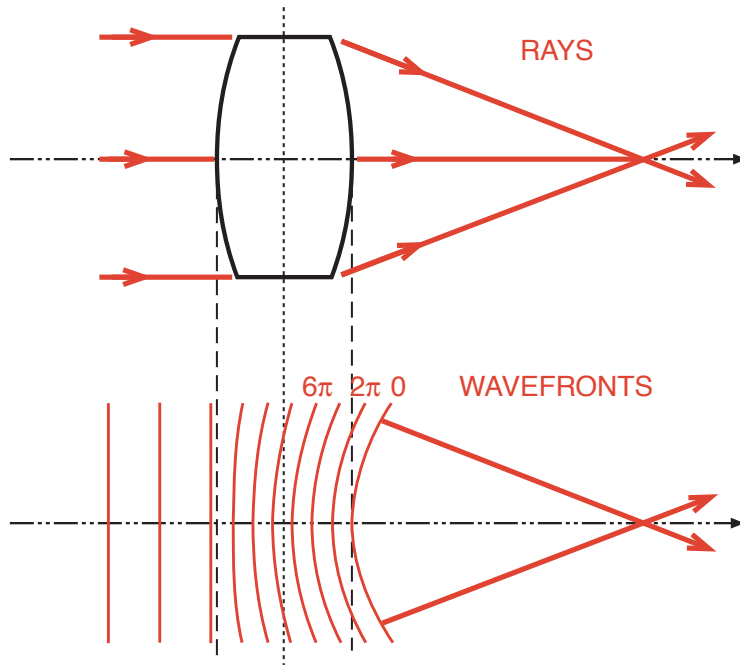


Figure 8: Positive lens with rays (upper) and wavefronts (lower). The converging wavefronts are labelled with phase corresponding to HTD of $\exp(i\omega t)$ dependence

$$\Phi_1(\rho) = k_o \sum n l_n \quad (74)$$

in which n is the glass index of refraction and $k_o = 2\pi/\lambda_o$, where λ_o is the free space wavelength.

Assuming a spherical R_1 (which can be refined in the next section), one can write the departure δ as is well-known:

$$\delta = R_1 - \sqrt{R_1^2 - \rho^2} \quad (75)$$

Then the phase delay $\Phi(\rho)$ is given by

$$\Phi_1(\rho) = k_o \delta + n k_o h(\rho). \quad (76)$$

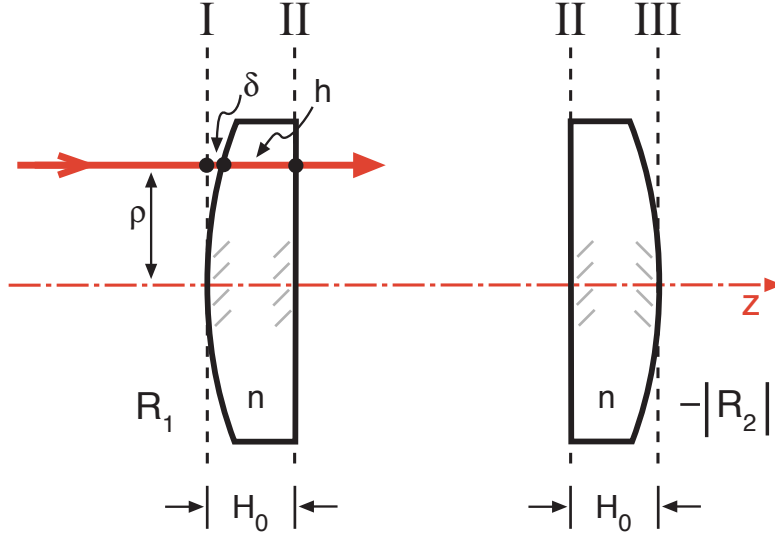


Figure 9: Notation for plano-convex lens with central thickness H_o . Calculation of phase delay at red ray δ in air and $h(\rho)$ in glass.

Combining Eq. (75) and (76) assuming $\rho/R_1 \ll 1$ yields the approximate form:

$$\Phi_1(\rho) = -k_o(n-1)\frac{\rho^2}{2R_1} + nk_oH_o \quad (77)$$

in which H_o is the thickness of the lens at $\rho = 0$.

In Fig. 9 we form a double-convex lens by placing the two lens elements together. Now in forming the overall transmission function, it is asserted that this is simply the product of the two transmission functions. The details follow.

For the second lens, let us be careful with signs, i.e.,

$$\Phi_2 = -k_o(n-1)\frac{\rho^2}{-2|R_2|} + nk_oH_o. \quad (78)$$

And since R_2 itself is negative. we rewrite Eq. (78) as follows:

$$\Phi_2 = -k_o(n-1)\frac{\rho^2}{2R_2} + nk_oH_o. \quad (79)$$

Hence, by the defining expression in Eq. (72), we form the product of the transmission functions corresponding to Eqs. (77) and (79). Moreover, the thin lens approximation is to set $H_o = 0$. Hence, the sum of Eqs. (77) and (79) yields the thin lens approximation for the phase delay. The corresponding transmission function for the double-convex lens is given by substitution of Eqs. (77) and eqrefeq79 with $H_o = 0$ into Eq. (73). Thus, the derivation yields the transmission function as follows:

$$T(\rho) = e^{ik_o\frac{(n-1)}{2}\rho^2\left(\frac{1}{R_1} - \frac{1}{R_2}\right)} \quad (80)$$

With the positive lens one needs to have a positive focal length. From Eq. (80) and comparing to Eq. (70), clearly one has

$$\frac{1}{f} = (n-1)\left(\frac{1}{R_1} - \frac{1}{R_2}\right) \quad \text{and} \quad (81)$$

$$T(\rho) = e^{+ \frac{ik_o\rho^2}{2f}}.$$

Lets look at the sign in Eq. (81). It tells us that the phase of the "forward-curved" wave in the output is bent forward as is clear from Fig. 8. This sign for the transmission function is in accord with an $exp(i\omega t)$ notation.

4.2 Generalized transmission function for aspheres

The transmission model for a lens as given in Sec. 4.1 is based on a mixture of ray and wave optics. It has the advantage of building a good physical understanding of the performance of a lens, but it does not give much insight into what would constitute an ideal shape for a lens nor on what would lead to a lens of idealized performance. For Fourier optics one needs a more abstract definition of a lens that is based on diffraction theory. This formulation also should not be based on the assertion of simple spherical surfaces. With today's knowledge we understand that some aspherical surface is needed if one is planning excellent performance.

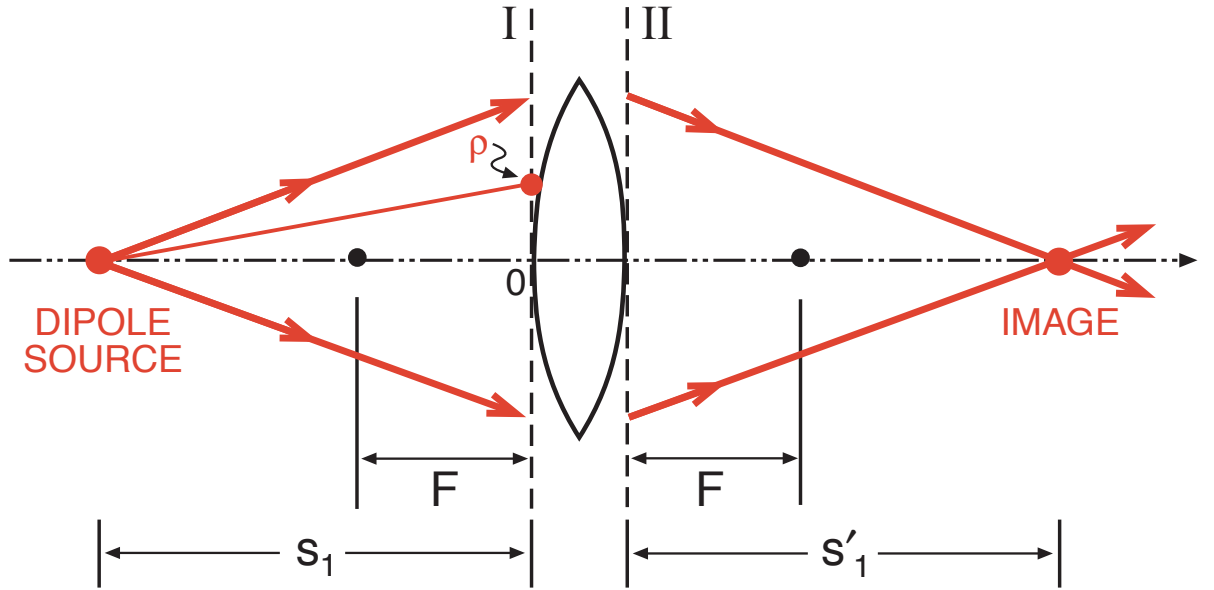


Figure 10: Transmission function for imaging the point source with an asphere, see Eqs. (82) to (85)

For the Fourier optics model, we prefer to start with a result or foundation based on Maxwell's equations. So assume a monochromatic plane-polarized light from a laser of wavelength λ . From Eq. (33) for a delta function input point source at a distance s_1 from the lens in Fig. 10, one can immediately write the expanding wavefront at plane I, $E_x(\rho)$ given by $\exp(-ik\sqrt{s_1^2 - \rho^2})$ where apodization is dropped.

Now a few examples and some reflection leads one to an answer of the following question. What exiting wavefront will lead to a point source at a distance s'_1 from plane II? Of course it will likely be blurred by diffraction.

The answer is that the exiting wavefront from plane II needs to have a wavefront given by $\exp(ik\sqrt{s_1'^2 + \rho^2})$. Again we have neglected the possibility of using apodization.

The transmission function for a lossless aspheric lens $T(\rho)$ is then defined with a phase delay or sag factor $\Phi(\rho)$, as follows:

$$T(\rho) = \frac{\text{Scalar electric field exiting plane II}}{\text{Scalar electric field entering plane I}} \quad (82)$$

$$T(\rho) = e^{-i\Phi} \quad (83)$$

$$T(\rho) = \frac{e^{+ik[(s_1'^2 + \rho^2)^{1/2} - s_1']}}{e^{-ik[(s_1'^2 + \rho^2)^{1/2} - s_1]}}, \quad (84)$$

in which the radius $\rho = \sqrt{x^2 + y^2}$ in the transverse plane as in Fig. 10. We have made the lens thin by introducing the subtraction terms s_1' and s_1 , in the numerator and denominator, respectively. The transmission of Eq. (84) is expanded in terms powers of $(\rho/s_1')^{2m}$ and $(\rho/s_1)^{2m}$ using G & R: 1.112 to yield

$$T_b(\rho) = e^{ik \left(s_1' \left[\frac{1}{2} \left(\frac{\rho}{s_1'} \right)^2 - \frac{1}{8} \left(\frac{\rho}{s_1'} \right)^4 + \frac{1}{16} \left(\frac{\rho}{s_1'} \right)^6 - \frac{5}{128} \left(\frac{\rho}{s_1'} \right)^8 + \dots \right] + s_1 \left[\frac{1}{2} \left(\frac{\rho}{s_1} \right)^2 - \frac{1}{8} \left(\frac{\rho}{s_1} \right)^4 + \frac{1}{16} \left(\frac{\rho}{s_1} \right)^6 - \frac{5}{128} \left(\frac{\rho}{s_1} \right)^8 + \dots \right] \right)} \quad (85)$$

Eq. (85) is a complete specification for an asphere in a power series expansion. While a complete discussion of this transmission function is beyond the scope of this article, more details can found in the literature [13]. Detailed aberration theory references are also cited [12, 14, 15].

4.3 Illustrative design of the tailored asphere

In optical system design it is commonplace to design aspheric lenses using modern digital computer software. Large apertures are readily handled. Moreover, a lens specification in terms of phase delay as the $\phi(\rho)$ in Eq. (82) to (85) is readily manufactured. This specification based on Fourier optics and wavefronts makes an important connection of Fourier optics to geometric optics or optical system design.

Axicons are lens elements having the property of transforming a point source of light into an axial segment, i.e., increasing the depth of field. In

such an application one typically has a range of focal lengths to accommodate, call it $f(\rho)$. If one proposes to create a lens design with a radially symmetric aspheric lens, it is necessary to establish an appropriate phase delay $\Phi(\rho)$ and a corresponding transmission function, $T_a(\rho)$ for the lens maker.

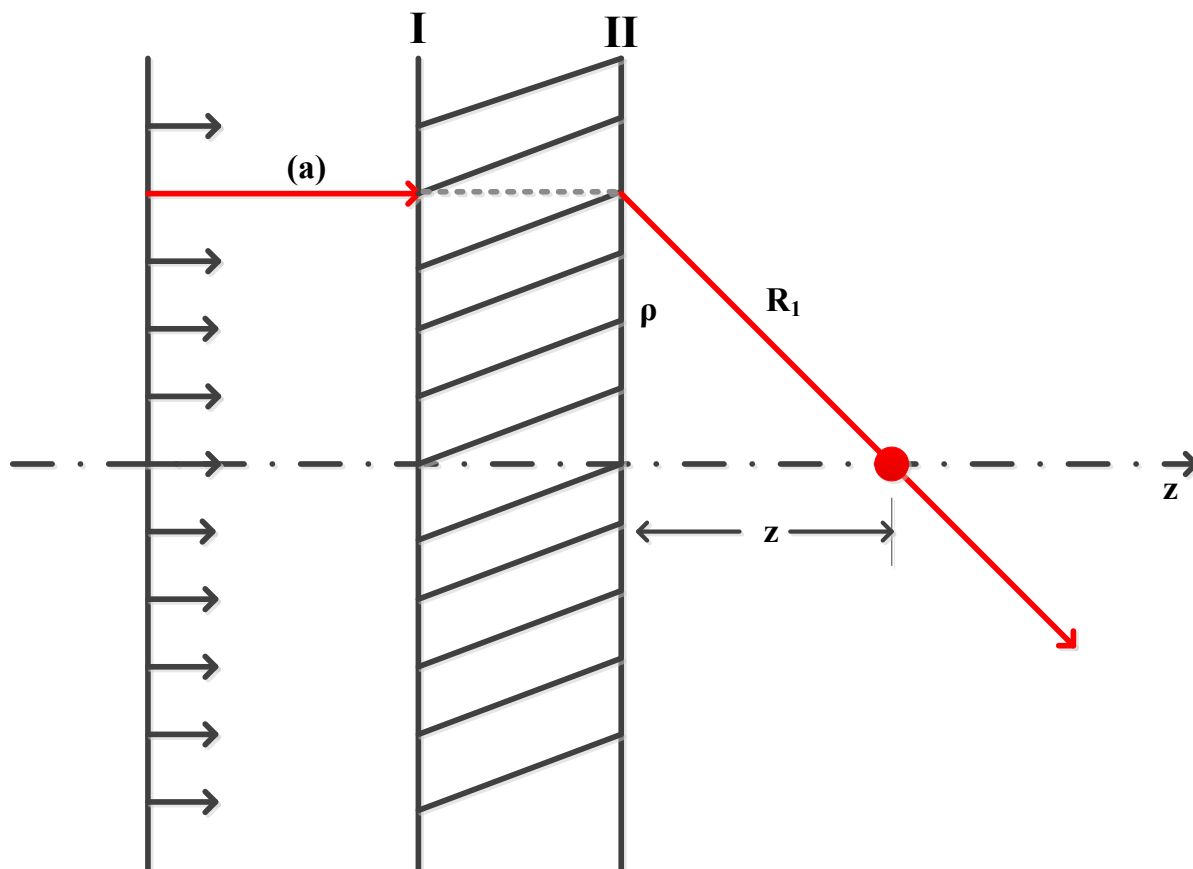


Figure 11: Aspheric lens $\Phi(\rho)$ between planes **I** - **II** with plane wave incident. Ray (a) has an effective focal length shown as z .

In the following paragraphs of this section, we describe the design of an asphere given a desired radial variation in focal length using Fourier optics wavefront notions. More specifically, we wish to establish the relationship between $\phi(\rho)$ and the corresponding radially varying focal length $f(\rho)$, as

in Fig. 11. This is a basic question.

Consider the asphere is between planes **I**, **II**. A plane polarized plane wave is incident. Rays at different heights are refracted to the optical axis crossing at different values z for each ray. Clearly the problem is ideally suited to our Rayleigh-Sommerfeld-Smythe formulation.

Choosing Eq. (33) and recognizing that the phase term $\exp(-ikR_1)$ is controlling, we write the reduced form for the axial field, E_x :

$$E_x(0,0,z;\nu) = ik \int_{II} E_x(\rho,z;\nu) \frac{e^{-ikR_1}}{R_1^2} z \rho d\rho \quad (86)$$

in which $R_1 = (\rho^2 + z^2)^{1/2}$. Clearly the exiting E_x is given by

$$\begin{aligned} E_x(\rho,z;\nu) &= T(\rho)E_o \text{ or} \\ E_x(\rho,z;\nu) &= E_o e^{-i\phi(\rho)} \end{aligned} \quad (87)$$

Substitution of Eq. (87) into Eq. (86) yields the following integration:

$$E_x(0,0,z;\nu) = ikE_o \int_{II} \frac{e^{-i(\phi(\rho) + kR_1)}}{R_1^2} z \rho d\rho \quad (88)$$

Stationary phase is used to evaluate this integration and to find the $z = f(\rho)$ for the ray (a) in Fig. 9. Hence, one has

$$\frac{d\phi(\rho)}{d\rho} + \frac{k\rho}{(\rho^2 + z^2)^{1/2}} = 0. \quad (89)$$

Substitution of $z = f(\rho)$ into Eq. (89) gives a basic result:

$$\frac{d\phi(\rho)}{d\rho} = \frac{-k\rho}{(\rho^2 + f^2)^{1/2}}. \quad (90)$$

Clearly, if one is given a specification for the focal length of the lens, Eq. (90) is readily integrated, say numerically, to find the $\phi(\rho)$ as required.

When one wishes to find the focal length $f(\rho)$ given the slope in the phase delay, $\phi'(\rho)$, Eq. (90) is readily rewritten, as follows:

$$f(\rho) = \pm \left[\left(\frac{k\rho}{\phi'(\rho)} \right)^2 - \rho^2 \right]^{1/2} \quad (91)$$

As a practical point about this synthesis procedure, it is remarked that physically one can in general develop a specification $f(\rho)$ and then compute $\phi(\rho)$ for the lens design. Tailoring the design by directly adjusting $\phi(\rho)$ is not practical since the total phase is very large, say 1000 radians, and the tailoring needed is small [13].

4.4 The paraxial approximation for a lens transmission function

In Sec. 4.2 the ideal transmission function is defined by Eq. (82) and (84). Then, neglecting possible apodization means, we describe an ideal lens by the transmission function, Eq. (85) using the Maxwell based results for propagation into the right-half-space. It is particularly important to take note of the fact there is no paraxial limit in any of this.

A simple binomial expansion in terms of $(\rho/s)^2$ is known to converge when this term is less than unity. Thus, in high quality diffraction-limited design, it is not unusual to go out to the tenth power of (ρ/s) . Practical examples of combining modern lens design software with Fourier optics techniques occur in the literature [13].

For an introduction to Fourier optics, it is typical to base the deductions mainly on illustrations drawn from far-zone and Fresnel thinking. Hence, herein, we would like to make this connection as well.

Clearly as ρ/s_1 and ρ/s'_1 become small, Eq. (85) can be approximated by retaining only the first members. Hence, the paraxial form for the transmission function is given by

$$T_p(\rho) = e^{i\frac{k}{2}\rho^2\left(\frac{1}{s_1} - \frac{1}{s'_1}\right)} \quad (92)$$

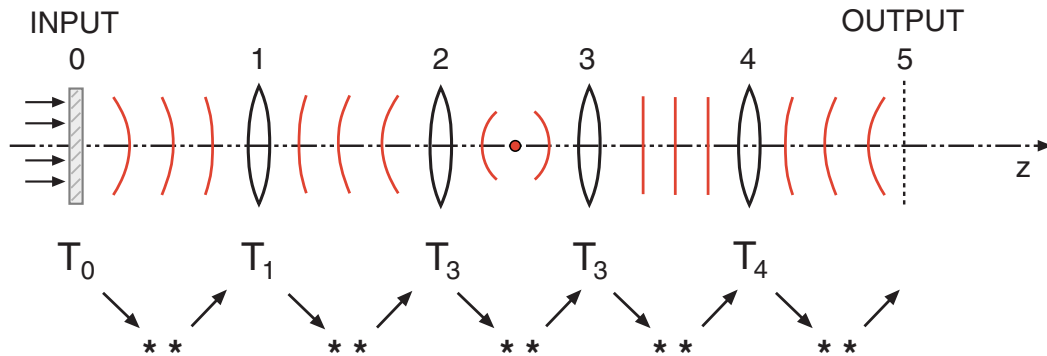
Equation (92) provides a nice confirmation of the signs seen in Eqs. (80) and (81).

5 Cascade of lenses & impulse response

The cascade of lenses shown in Fig. 12 is one of the central topics in Fourier optics. For definiteness in this linear system, consider four simple thin lenses (1 to 4) with an input transparency (0) illuminated by a

FOURIER PHYSICAL OPTICS - SUMMARY

CALCULATION OF OUTPUT WAVES



LIGHT IS PROPAGATING FROM LEFT TO RIGHT

TRANSMISSION THRU LENS ... PRODUCT
FREE SPACE PROPAGATION ... CONVOLUTION

Figure 12: Cascade of 4 lenses for imaging input to plane 5. This is a central topic in Fourier optics to compute the impulse response p_{05} for the cascade

monochromatic plane wave with its electric field along the x -axis. Propagation of light in the open spaces 0 to 1, 1 to 2, ... and 4 to 5 can be analyzed by repeated applications of the Sec. 3.3 Fresnel zone means or by Eq. (33) the exact expression. The double asterisks stand for the two-dimensional convolutions over the transverse planes. And of course the transmissions through each lens are treated by products using $T_1(\rho)$, $T_2(\rho)$ and so on, as described in Sec. 4.

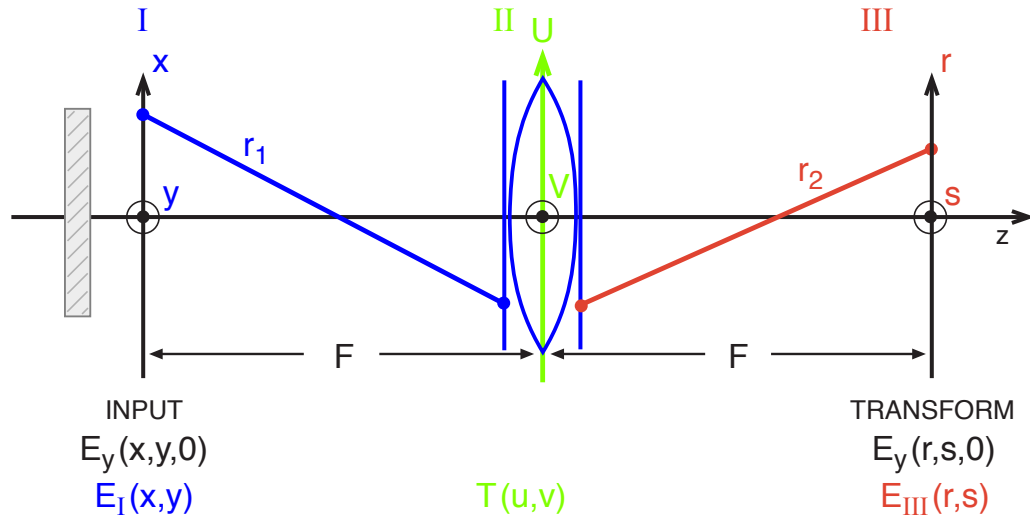


Figure 13: The optical Fourier transform configuration. From two Fresnel zone calculations, one finds an ideal Fourier transform in plane III for the input $E_I(x, y)$.

6 The optical Fourier transform

Consider the configuration with an illuminated picture in plane I (x, y) , a lens of focal length F in plane II (u, v) , and an output plane III (r, s) as shown in Fig. 13. The Fresnel zone calculation is given in detail with a color code corresponding to the figure. The reader is invited to fill in the missing details in this computation after a careful study of the color code in Fig. 13 compared with Eqs. (93) through (97). Equation (96) is a major result.

For the Fresnel zone calculation:

$$E_{II} = e^{\frac{ik(u^2 + v^2)}{2F}} \frac{ike^{-ikF}}{2\pi F} \iint_{-\infty}^{\infty} dx dy E_I(x, y) e^{-\frac{ik}{2F}[(u-x)^2 + (v-y)^2]} \quad (93)$$

$$E_{III} = \frac{ike^{-ikF}}{2\pi F} \iint_{-\infty}^{\infty} dudv E_{II}(u,v) e^{-\frac{ik}{2F}[(u-r)^2 + (v-s)^2]} \quad (94)$$

$$\text{Integrate using } \int_{-\infty}^{\infty} due^{-\frac{ik}{2F}[u-(r+x)]^2} = (1-i)\left(\frac{\pi F}{k}\right)^{1/2} \quad (95)$$

$$E_{III} = \frac{ie^{-i\frac{2\pi 2F}{\lambda}}}{\lambda F} \iint_{-\infty}^{\infty} dx dy E_I(x,y) e^{i2\pi \frac{1}{F\lambda}[rx + sy]} \quad (96)$$

$$\text{in which } f_x = \frac{-r}{F\lambda} \text{ and } f_y = \frac{-s}{F\lambda}. \quad (97)$$

7 The optical transform hybrid processor

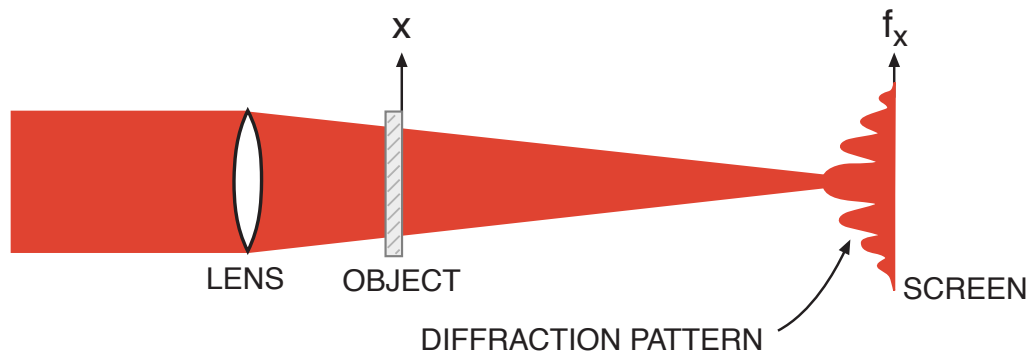
As shown in Fig. 13 and Sec. 6, the F to F spacing provides an ideal Fourier transform in amplitude of the scalar electric field, E_x in Eq. (96). There is a phase delay due to the propagation distance ($2F$). This configuration has a singular position in Fourier optics, since it enables, the study and visualization of the optical Fourier transform of various complicated objects.

In learning Fourier transform theory, the function $g(x,y)$ and its associated pair $G(f_x, f_y)$ are studied, but there is no "alignment" described between axes x, y with those in transform space, i.e., with f_x, f_y . Mathematically, this is a correct point of view, since the function space (x, y) and the Fourier space (f_x, f_y) are not in the same domains.

However practice develops some handy points of view; and in optical transform configurations, the x, y plane is generally parallel to the f_x, f_y plane; and the respective axes are collinear, i.e., x with f_x and y with f_y . The handy rules of thumb which we use on patterns in function space in order to describe their corresponding patterns in transform space are summarized in Fig. 14. These rules have proven very helpful in the development of diffraction pattern sampling. Several optical-transform-hybrid processors have been developed using a front-end lens and some form

WHAT IS A DIFFRACTION PATTERN

$$G(f_x, f_y) = \int_{-\infty}^{\infty} \int_{-\infty}^{\infty} dx dy g(x, y) e^{-i2\pi(f_x x + f_y y)}$$



- EDGES YIELD SPIKES
- EDGE ANGLE CORRELATIONS RETAINED
- INVERSE SPACE-FREQUENCY RELATIONSHIP
- TRANSLATIONAL INVARIANCE

Figure 14: The basis of diffraction-pattern-sampling for pattern recognition in optical-electronic processors is summarized in 4 rules

of photodetector array placed in the back focal plane. Commonly used are the linear photodiode array, the CCD, the CMOS, and the ring-wedge detectors [16, 17].

One more practical point to mention is that photodetectors are sensitive to the energy density in the electric field, i.e., proportional to $\mathbf{E} \cdot \mathbf{E}^*$. This includes vision, film cameras, and the digital cameras. So in Eq. (96) of Sec. 6, the $|E_{III}|^2$ is reading the Fourier transform squared. The practical laboratory point is that in an optical setup with a laser illumination if you find one position where there is a broad spot of illumination followed by another position where the illumination narrows to a tiny point, you have found excellent positions for an object transparency and its optical Fourier

transform intensity, respectively. There are scale factors involved, and you might make up a problem set to find them. They have been purposely omitted in the equation of Fig. 14. In practice the object is slid along the optical axis and the transform pattern recorded at the detector becomes smaller as the distance decreases.

7.1 The ring-wedge photodetector [16]

For sampling the Fourier transform intensity, an interesting hybrid processor uses a photodiode array that is divided into two 180° portions. In one portion, there are 32 pie-shaped wedges; and on the other half, there are 32 annular rings. These choices were based on providing as fine a sampling as is necessary for pattern recognition of very fine grained photographs or for particulate analysis.

With particulate analysis the quantitative study did not progress very well using lasers due to the difficulties with speckle. As the understanding of speckle progressed, it became clear that the annular detector rings are ideally suited for averaging out the variations caused by speckle and excellent for measuring histogram-like patterns even with complicated mixtures of size distributions.

In pattern recognition it is an interesting question to wonder why would one use a Fourier transform base of data rather than the original object's pixel data. There is probably no simple answer; but clearly system-wise, one method of approach may be vastly simpler. Also if one can get data down early in the system, as from one-million pixels to thirty-two, that is likely to be advantageous [17].

In Fig. 15, the three illustrations on this page show (left) the optical transform of a sharp hypodermic needle, (middle) a hypodermic needle with a defective tip, and (right) the optical transform to the defective needle. Commercially, this sensitivity of the transform pattern to edge and tip defects is used as the basis for production testing of disposable hypodermic needles. The commercial system can make operator-independent quality assessment at the rate of one inspection per millisecond. Moreover, the testing is non-destructive and it can be done in a clean-room.

Related literature appears on diffraction pattern sampling in white light [18] and the ring-wedge detector and neural networks [19], particulate sizing [20] and image quality [21].

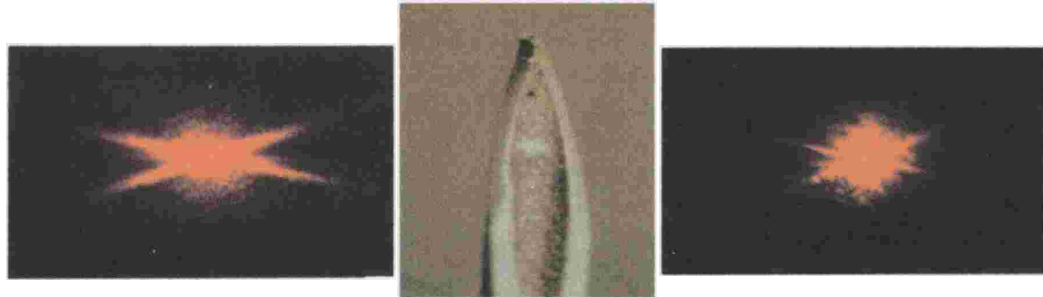


Figure 15: Rapid, millisecond testing of quality of sharpness of hypodermic needles (2.5 billion needles per year) is accomplished with the ring-sedge optical transform
 hybrid: (left) excellent quality; poor needle; poor transform.

8 Canonical optical processor - the 4F system

In Fourier optics, the Fourier optical transform configuration is a cornerstone of the subject both as a theoretical achievement and a practical system that is application relevant. Equally central to Fourier optics is the cascade of two Fourier transform configurations. As shown in Fig. 16, at the close of this section, we have used a focal length F_1 for the first lens, then a stop and filter transparency $P(u, v)$ at plane **II** followed by a second lens of focal length of focal length F_2 and an output plane **III**(r, s). Separate labeling of the transverse coordinates has been used for clarity.

Clearly for a two lens cascade, we can analyze it for the output at plane **III**. With just a circular stop in plane **II**, we need first to recognize that the output plane **III** is an image plane of **I**. And the image is inverted and magnified in the ratio of $-F_2/F_1$.

Study of this system is useful in the explanation of imaging and diffraction limitations in imaging simply by considering rect or circ function apertures for the transmission function $P(u, v)$. This system is shown at the end of this section in Fig. 16, together with final equations resulting from the derivation of the following paragraphs. Also, the fundamental concepts of

optical information processing can be learned by considering the various filtering operations that are possible with appropriate choices of the mask $P(u, v)$.

Using the results of the calculation for a single Fourier-section in Sec. 6, we can immediately write an expression for the scalar component in plane III, $E_3(r, s)$, in terms of the input at plane I: $E_1(x, y)$ and the transmission mask $P(u, v)$. The notation for the transverse plane coordinates is I (x, y) , II (u, v) , and III (r, s) . These coordinates are chosen with different symbols so that the integrals over planes I and II can be regrouped, as shown, without confusion.

With monochromatic illumination and for an arbitrary input [both incorporated in the function $E_1(x, y)$], we see that the output $E_3(r, s)$ is obtained by completing a convolution-like integration of $E_1(x, y)$ with an impulse-response kernel. To make this linear system form more evident, we define the impulse response $p(r + F_2x/F_1, s + F_2y/F_1)$ by Eqs. (98) and (99), as follows:

$$p\left(r + \frac{F_2}{F_1}x, s + \frac{F_2}{F_1}y\right) = \frac{e^{-i\frac{4\pi}{\lambda}(F_1 + F_2)}}{F_1/F_2} \iint_{-\infty}^{\infty} df_r df_s P(u, v) e^{-i2\pi[f_r(r + \frac{F_2}{F_1}x) + f_s(s + \frac{F_2}{F_1}y)]} \quad (98)$$

in which the spatial frequency variable f_r, f_s are

$$f_r = \frac{-u}{F_2\lambda} \quad \text{and} \quad f_s = \frac{-v}{F_2\lambda} \quad (99)$$

The output $E_3(r, s)$ is given in terms of the impulse response $p(r, s)$ as follows in Eq. (100):

$$E_3(r, s) = \iint_{-\infty}^{\infty} dx dy p\left(r + \frac{F_2}{F_1}x, s + \frac{F_2}{F_1}y\right) E_1(x, y). \quad (100)$$

In this manner we derived the important linear system result which expresses the output of the lens-filter-lens cascade in the convolution-like form of the input $E_1(x, y)$ with the impulse response $p(r, s)$. Moreover, we have obtained an explicit formula for the function $p(r, s)$ in terms of the lens-filter configuration.

Impulse Response: The following illustrative example serves to clarify the language impulse-response. Consider the canonical processor to be illuminated by a delta-like pinpoint of light at the position $x = x_o, y = y_o$. What is the output in plane **III**? From the general result, substitution of $E_1(x, y) = \delta(x - x_o, y - y_o)$ and integration yield the result shown in Eq. (101), viz.,

$$E_{3\delta}(r, s) = p\left(r + \frac{F_2}{F_1}x_o, s + \frac{F_2}{F_1}y_o\right) \quad (101)$$

The system is said to be space-invariant.

Spatial-Frequency Scaling: For simple pupil-like masks in plane **II**, the canonical processor will form an image in plane **III** of an object in plane **I** with a magnification of $(-F_2/F_1)$. In the derivation above, frequency scaling is with respect to the output plane **III**.

In general, however, spatial frequency scaling can be done either with respect to output plane coordinates using Eq. (102):

$$f_r = \frac{-u}{F_2\lambda} \quad \text{and}; \quad f_s = \frac{-v}{F_2\lambda} \quad (102)$$

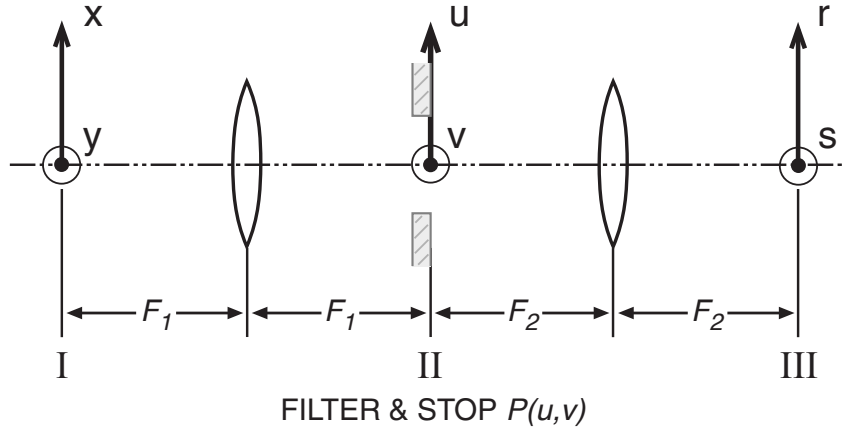
or with respect to input plane coordinates using Eq. (103):

$$f_x = \frac{-u}{F_1\lambda} \quad \text{and}; \quad f_y = \frac{-v}{F_1\lambda} \quad (103)$$

From Eq. (100) to (103) we write the output scalar electric field in terms of the input. This result is accurate to the Fresnel zone accuracy with all phase terms retained in Eqs, (104) and (105). With all phase terms retained, as before:

$$E_3(r, s) = \frac{-e^{-i\frac{4\pi}{\lambda}(F_1 + F_2)}}{\lambda^2 F_1 F_2} \iint_{-\infty}^{\infty} dx dy E_1(x, y) \bullet \iint_{-\infty}^{\infty} dudv P(u, v) e^{i2\pi \left[\frac{u}{\lambda F_2} \left(r + \frac{F_2}{F_1} x \right) + \frac{v}{\lambda F_2} \left(s + \frac{F_2}{F_1} y \right) \right]} \quad (104)$$

CANONICAL OPTICAL PROCESSOR



I. OBJECT PLANE	$E_1(x,y;\nu)$
II. TRANSFORM PLANE	$P(u,v;\nu)$
III. IMAGE PLANE	$E_3(r,s;\nu)$

Figure 16: The 4-F optical processing provides both an idealized space-invariant image as well as a perfect optical Fourier transform. It is useful both in theoretical calculations and in laboratory.

or

$$E_3(r,s) = \iint_{-\infty}^{\infty} dx dy E_1(x,y) \left\{ \frac{-e^{-i\frac{4\pi}{\lambda}(F_1+F_2)}}{F_1/F_2} \cdot \right. \\
 \left. \cdot \iint_{-\infty}^{\infty} d\left(\frac{u}{\lambda F_2}\right) d\left(\frac{v}{\lambda F_2}\right) P(u,v) e^{i2\pi \left[\frac{u}{\lambda F_2} \left(r + \frac{F_2}{F_1} x \right) + \frac{v}{\lambda F_2} \left(s + \frac{F_2}{F_1} y \right) \right]} \right\} \quad (105)$$

From Eqs. (100) to (103) we write the output scalar electric field in terms

of the input. This result is accurate to the Fresnel zone accuracy with all phase terms retained in Eqs. (104) and (105).

9 Summary

The article on Fourier optics and electromagnetic waves provides a readable, concise, and rigorous treatment that will be clear and understandable without particular experience or background. There are 8 separate sections starting with a discussion of Maxwell's equations in real-valued time dependent form. Then in Sec. 1.2, the standard notation of the Fourier transform and its inversion is defined. The signal representation is explained and summarized in Fig. 1.

Section 2 treats the central problem of propagation into the right-half-space. The rigorous explanation of the integral expression goes by the name Rayleigh-Sommerfeld-Smythe. The addition of the Smythe name is mine (N. George) because his rigorous theory has clarified what is often confusing in the optics literatures. The basic equations are summarized in Eq. (33) to (36).

To make the material readable and interesting for the theorist who is not experienced with Optics, we are very careful with the choice of the first illustrative problem. In Sec. 3.1, it is the exact calculation of the radiation along the optical axis [10] from a circular aperture. As an exact calculation, it serves as an excellent choice for the student to really think about, There is little or no jargon as well.

Then, in Sec. 2 the far-zone is treated using the far-zone approximation that is not paraxially limited. Section 3.3 has the standard Fresnel zone coverage. Section 4 contains a thorough discussion of lenses from the wavefront point of view. This is Sec. 4.2. Fairly recent thinking about aspheres is presented together with an explanation of how to go from wavefront delay ϕ to focal length f in Eq. (90). Whenever possible the Fourier optics or wavefront presentation is made without paraxial approximations. It does seem that future applications with the use of digital computers will greatly expand the practicality of optical system design using Fourier optics.

In the later sections of the article, we describe some important illustrations of Fourier optics. This includes the ideal F to F optical Fourier transform and then the 4F canonical processor. If you see errors or mistakes, my apologies, please send me an email: ngeorge@optics.rochester.edu.

References

- [1] Duffieux, P.M., *The Fourier Transform and Its Applications to Optics*. (English translation: Second edition) Masson, Editeur, Paris (1970)
- [2] Goodman, J.W., *Introduction to Fourier Optics*. McGraw-Hill, New York, 1st Edition (1968) & 3rd Edition (2004)
- [3] Papoulis, A., *Systems and Transforms with Applications in Optics*. McGraw-Hill, New York (1968)
- [4] Griffiths, D.J., *Introduction to Electrodynamics*. Second Edition, Prentice Hall, New Jersey (1989)
- [5] Papas, C.H., *Theory of Electromagnetic Wave Propagation*. McGraw-Hill, New York (1965)
- [6] Balanis, C.A., *Advanced Engineering Electromagnetics*. John Wiley & Sons, New York (1989)
- [7] Kong, J.A., *Electromagnetic Wave Theory*. EMW Publishing, Cambridge (2008)
- [8] Smythe, W.R., *Static and Dynamic Electricity*. 3rd Edition, Revised Printing, Taylor & Francis (1989)
- [9] Smythe, W.R., *The Double Current Sheet in Diffraction*. Phys. Rev. 72, 1066 (1947)
- [10] English, R.E., Jr., and George, N., *Diffraction from a circular aperture: on-axis field strength*. Appl. Opt. **26** (12), 2360-2363 (1987)
- [11] Jackson, J.D., *Classical Electrodynamics*. Third Edition, John Wiley & Sons, New York (1999)
- [12] Born, M., and Wolf, E. *Principle of Optics*. Pergamon Press, New York (1959)
- [13] George, N., and Chen, X., *Extended Depth-of-Field Lenses and Methods for Their Design, Optimization and Manufacturing*. U.S. Patent Application Publication US2010/0002310 A1 (2010)

- [14] Kidger, M.J., *Fundamental of Optical Design*. SPIE Press Monograph, PM 92 (2001)
- [15] Welford, W.T., *Aberrations of the Symmetrical Optical System*. Academic Press (1974)
- [16] George, Nicholas; J.T. Thomasson, *Photodetector Light Pattern Detector*. U.S. Pat. No. 3,689,772 (1972)
- [17] George, Nicholas; Niels Jensen; J.T. Thomasson, *Diffraction Pattern Sampling for Real-Time Pattern Recognition*. J. Opt. Soc. Am.; 1380A (1972)
- [18] Wang, Shen-ge; N. George, *Fresnel zone transforms in spatially incoherent illumination*. Appl. Opt, **24**, pp. 842-850 (1985)
- [19] N. George; Wang, Shen-ge; and D.L. Venable, *Pattern recognition using the ring-wedge detector and neural network software*. SPIE 1134 (1989)
- [20] Coston, S.D; N. George; *Particle size inversion*. Appl. Opt. **30**, pp. 4786-4794 (1991)
- [21] Bertanger, D.M.; N. George, *All digital ring-sedge detector applied to automatic image quality assessment*. Appl. Opt. **39**, pp. 4080-4097 (2000)

About the author

Nicholas George

Joseph C. Wilson Chair Professor of
Electronic Imaging & Professor of Optics
Phone: 585-275-2417 Cell: 585-329-1029
Email: ngeorge@optics.rochester.edu
The Institute of Optics, University of Rochester



Nicholas George is the Joseph C. Wilson Professor of Electronic Imaging and a Professor of Optics at the University of Rochester. He was the founding Director of the Center for Electronic Imaging Systems (CEIS), funded in part by the National Science Foundation under the S/IUCRC program, and also of the highly rated ARO-URI Center for Opto-Electronic Systems Research. Prior to this he was Director of The Institute of Optics at the University of Rochester for more than four years, serving during a period of unprecedented growth. Previously he was a Professor of Applied Physics and Electrical Engineering at the California Institute of Technology. He received the B.S. degree with highest honors from the University of California at Berkeley, the M.S. degree in Electrical Engineering from the University of Maryland, and the Ph.D. in Electrical Engineering and Physics from the California Institute of Technology. Presently he serves as Director of the Emerging Electronic Imaging Systems Laboratory. He has served as principal thesis advisor to 50 doctoral students who have gone on to responsible academic positions, R & D systems work, and leadership positions in industry and finance. His firsts and near-firsts in modern optics include the holographic diffraction grating, the holographic stereogram, the ring-wedge detector robotic vision system, the laser heterodyne for pollution sensing of nitrogen oxides, the infrared hologram, the theory and experiments for the wavelength dependence of speckle, the FM-FM laser line scan system for remote contouring of aerial maps, and the logarithmic asphere for extended depth of field cameras.